Microelectrode arrays with active-area geometries defined by spatial light modulation

Yan B. Vogel [a], Angela Molina [b], Joaquin Gonzalez [b, *], and Simone Ciampi [a, **]

[a] *School of Molecular and Life Sciences, Curtin Institute of Functional Molecules and Interfaces, Curtin University, Bentley, Western Australia 6102, Australia*
[b] *Departamento de Quimica Fisica, Universidad de Murcia, Murcia 30003, Spain*
[*]Corresponding author. *E-mail address: josquin@um.es*
[**]Corresponding author. *E-mail address: s.ciampi@curtin.edu.au*

ABSTRACT. Microelectrode arrays form the basis of electrochemical sensing devices because of their unique properties, such as enhanced mass transport and steady-state diffusion currents. However, they demand a predefined and rigid geometry, and require a connecting pad for each element of the array. Here it is reported the formation of microelectrode arrays whose geometry is defined by the shape of a light pattern projected on an unstructured silicon electrode. Spatiotemporally resolved fluxes of charge carriers are used to confine a model electrochemical reaction only to the illuminated areas. Using spatial light modulators, microelectrode geometry is adjusted instantaneously, at will, on a homogeneous semiconductor electrode carrying a single electrical connection. By developing a theoretical model to analyze the current−potential data, it is revealed within which limits spatial light modulation can be used to enhance, on silicon, the mass transport of a diffuse redox system.

Keywords: microelectrode arrays; semiconductor electrochemistry; spatial light modulation; light addressable electrochemistry; monolayers on silicon

1. Introduction

Spatial light modulators (SLM) are devices that impose some form of spatial modulation to a light beam. Originally developed as video projection devices for entertainment purposes, SLM are now used in areas as diverse as photolithography [1], microscopy [2], 3D printing [3], and micromanipulation [4]. More recently, SLM have found applications in electrochemical research: a spatially modulated light beam can confine electrochemical reactions at a specific microscopic location within a macroscopic semiconductor–electrolyte interface [5]. Light generates charge carriers in the semiconductor, and these are driven by the space-charge electric field towards redox species present at the solid–liquid interface, hence localizing the redox process in correspondence to the illuminated area (Fig. 1A) [5]. This principle served as platform to develop mask-free lithography techniques [6-8], and has been successfully applied to interrogate the redox activity of a surface [9, 10], to develop surface chips for the capture of rare cells [11], to generate chemical gradients [12], and as a light-driven DNA sensor [13]. However, no reports are yet available on methods to harness spatially structured light to generate transient microelectrode arrays on readily available (unstructured) semiconductive or photoconductive surfaces.

Microelectrode arrays, owing in large part to developments in the technology required for the fabrication of integrated circuitry, are now readily available, relatively inexpensive, and the core of several chemical sensing devices [14, 15]. They offer the advantages of miniaturized electrodes, such as fast response time and increased sensitivity [16], and when multiple units are organized in an array they open up to multi-analyte sensing and mapping of a redox environment [14, 15]. However, microelectrode arrays are not free from constrains: a considerable amount of space is lost between conductive pads or to fit bonding wires and, most importantly, the geometry of the array is fixed and predetermined by a choice made prior to the experiment.

Here we begin to address some of these shortcomings by exploring the use of spatially modulated light to define the active area of multiple microscopic sites across an unstructured silicon electrode. We explore the parallel aspects of light activated electrochemistry, specifically testing the possibility of generating microelectrode arrays that have no bonding wires, no conductive pads, and of unrestricted and dynamic geometry. Microelectrode arrays are transiently formed by projecting light patterns on a silicon–electrolyte interface using a ferroelectric liquid crystal on silicon micromirror device as SLM. Our current setup allows projecting visible light patterns with a spatial resolution of 4.5 µm (Fig. 1B). Specifically, we have studied the voltammetric current–potential behaviour of macroscopic electrodes, with a single electrical connection, where only microscopic band-shaped regions are illuminated. We demonstrate experimentally, and model theoretically, to what extent increasing the width of dark regions can fine-tune the overlap between adjacent diffusion fronts, hence defining the conditions under which cyclic voltammograms show a progressive transition from macro- to micro-electrode behaviour. Finally, by analysing two silicon allotropes we demonstrate that the extent of electrochemical confinement depends strongly on charge carriers' diffusion lengths.

2. Experimental

2.1 Chemicals and materials

Unless otherwise specified chemicals were of analytical grade and used as received. Sulphuric acid (Sigma-Aldrich, Puranal, 95–97%), ammonium fluoride (Sigma-Aldrich, Puranal, 40%,), hydrofluoric acid (Sigma Aldrich, 48%), and 1,8-nonadiyne (Sigma-Aldrich, 98%), were used in wafer cleaning, etching, and hydrosilylation procedures. Milli-Q water with a resistivity >18.2 MΩ cm, redistilled dichloromethane and 2-propanol were used for surface modification procedures and washings. Ferrocene (Sigma-Aldrich, 98%), tetrabutylammonium perchlorate (Sigma-Aldrich, 98%) and acetonitrile (Ajax Finichem, 99.7%) were used to prepare electrolytic solutions. Copper sulphate (Chem-Supply, 99.5%) and potassium sulphate (Ajax Finichem, 99%) were used to prepare the electrolytic solutions used for patterning experiments. Gallium–indium eutectic (Sigma Aldrich, 99.99%) was used to form an ohmic contact to the silicon electrode. Single crystal silicon wafers, 500 µm thick, were purchased from Siltronix (Archamps, France). The wafers were n-type (phosphorous-doped) Si(111), and p-type (boron-doped) Si(100), with a nominal resistivity of 8–12 Ω cm unless otherwise stated.

2.2 Preparation of the amorphous silicon substrates

Highly doped (0.001–0.003 Ω cm) p-type (boron-doped) Si(100) wafers were cleaned in an ozone chamber immersed for 3 min in a 5% hydrofluoric acid solution and then blown dry under a nitrogen flow. The amorphous silicon film was grown on Si(100) by plasma-enhanced chemical vapour deposition until reaching a thickness of 1 μm.

2.3 Surface functionalization

All silicon samples were chemically modified according to the following procedure. Substrates were rinsed with dichloromethane, 2-propanol and water, immersed for 10 min in a deoxygenated 40% aqueous NH_4F solution, washed with water and dichloromethane and then blown dry under a nitrogen flow. A few drops of 1,8-nonadiyne were then placed on the top of the sample, which was immediately contacted with a quartz slide to limit the evaporation of the diyne. Samples were then kept for 2 h under nitrogen in front of a 312 nm light source (Vilber, VL-215.M, 30 W nominal power output) positioned approx. 20 cm away from the sample. Samples were rinsed thoroughly with dichloromethane before analysis.

2.4 Direct measurement of electrochemical confinement

The extent to which the electrochemical reactions were confined in 2D to match the illumination pattern was assessed by scanning electron microscopy (SEM) analysis of Cu_2O patterns electrochemically deposited on silicon photocathodes. In brief, a line-shaped feature of known width was projected on a diyne-modified silicon substrate while applying a negative potential of −0.5 V (vs Ag/AgCl, KCl_{sat}). The electrolytic solution contained Cu_2SO_4 (50×10^{-3} M) and K_2SO_4 (0.5 M). The amount of charge transferred per unit of area was kept constant at 1 μC μm^{-2}. SEM images of the Cu_2O patterns were acquired on a Zeiss Neon 40EsB FESEM equipped with a Schottky field emission gun operating at 5 kV and a chamber pressure of ca. 4×10^{-6} mbar.

2.5 Voltammetry simulations

The analytical model developed to simulate cyclic voltammograms is based on that of Santangelo *et al.* [17], but expanded to account for the microelectrode and band geometries.

This model is described in detail in Section S2. Simulation experiments were written and performed in GFortran and Mathcad 14.

3. Results and discussion

3.1. Electrochemical switching by a light stimulus

Proving the formation of transient microelectrode arrays upon local illumination is the main purpose of this study. Therefore, we first proceeded to investigate the experimental conditions where a light stimulus becomes a "switch" of the electrode kinetics. To prevent anodic decomposition of the electrode, and to allow for reproducible electrochemical measurements across a wide potential window (*vide infra*), hydrogen-terminated silicon substrates were modified with a monolayer of 1,8-nonadiyne [18], which prevents silicon oxidation under positive voltages [19], but still allows for efficient electron transfer [7]. The ferrocene/ferrocenium (Fc/Fc^+) redox couple was chosen for its ideal and well-known electrochemical behaviour. In order to ensure minority carriers depletion under dark and at a potential required for a fast Fc oxidation, we selected lowly doped (LD) n-silicon with a flat band potential more negative than the formal redox potential of the Fc/Fc^+couple. The formal redox potential of the Fc/Fc^+ couple, measured on highly doped (HD) p-type Si(111) electrodes (*i.e.* metal-like electrodes), is around 0.2 V (vs Ag/AgCl/sat. KCl, Fig. S1A). The LD n-type Si(111) substrates have a flat band potential of −0.3 V (vs Ag/AgCl/Sat. KCl, Fig. S1B). Therefore under dark the LD n-type Si(111) electrode is depleted of charge carriers at the potential where Fc oxidation dominates the redox process. When the semiconductor is illuminated, electron–hole pairs are generated in the solid and holes, driven both by the space-charge layer (SCL) electric field and by a concentration gradient, are trapped by Fc molecules in solution, Fig. 2A. In order to confirm this, the potential was scanned in cyclic voltammetry experiments performed both under dark and under red light (Fig. 2B, symbols and solid line, respectively). Data in Fig. 2B reveal the flow of an electrochemical current only when the semiconductor is illuminated, indicating the redox reaction occurs at an appreciable rate only upon electrode illumination.

3.2 Cyclic voltammetry of freely diffusing redox species on a photoanode

The main characteristic of a microelectrode is its radial diffusion profile. This is reflected on an enhanced mass transport of diffusible redox species, which on a metal electrode results in a steady-state electrochemical current [20, 21]. However, the electrochemical behaviour of semiconductor electrodes differs substantially from that of metal electrodes [17, 22-25]. The potential drop across a semiconductor–liquid interface is distributed between the diffuse layer (DL) and the SCL, the latter extending inside the semiconductor (Fig. 2A). When an external potential is applied across the interface, a large fraction of this potential can drop inside the SCL. In contrast, in a metal any applied bias drops exclusively across the diffuse layer [17, 22-25].

Because of these differences in the potential profile along the interface, the voltammetric responses of semiconductors and metals differ considerably [17, 22-25]. We therefore developed a theoretical model based on that of Santangelo *et al.* [17] in order to describe, and analyze, voltammetric photocurrent–potential curves of our silicon electrodes (see Section S2, for a full description of the model). Our model differs from that of Santangelo *et al*. in that it takes into account the geometry of the electrode, allowing for the interpretation of voltammetric responses of microelectrodes and microelectrode arrays.

Fig. 2C shows the theoretical influence of photocurrent magnitude on the voltammetric responses expected for freely diffusing redox species on a photoanode. At low photocurrent values, a steady state current is observed in the forward scan because the reaction kinetics is limited by the availability of photogenerated carriers. A stationary state arises because all photogenerated carriers are being consumed by the available electroactive species. This situation is for example experimentally observed when the light intensity is sufficiently low

(Fig. 2D). However, the same response could also arise when the illuminated area gets sufficiently small (*vide infra*). Therefore, one has to exert caution when trying to interpret steady state currents at photoelectrodes. In fact, the voltammetric curves at low photocurrent values resemble that of a metal electrode under radial or convective mass transport, such in the case of a microelectrode (Fig. S2) or a rotating disk electrode, respectively [20]. Because our principal aim is to demonstrate the formation of microelectrode arrays on semiconductors, a correct interpretation and analysis of the current–potential relationship is fundamental.

3.3 Voltammetric photocurrent–potential behaviour of freely diffusing Fc/Fc^+ on Si(111) electrodes under local illumination

The digital simulations of Fig. S2 show voltammetric curves of diffusing redox species on a metallic single band microelectrode as a function of the width of the band (*w*). As the band gets narrower, simulations anticipate a semi-stationary current and a progressive increase in current density. We then performed digital simulations for a single band photoanode microelectrode, again as a function of *w* (Fig. 3A and Section S2). Similarly to a metal electrode, there is an increase in current density as *w* decreases. However, a steady state current emerges when the band is sufficiently broad, a situation exactly opposite to a metal electrode. As pointed in the previous section, this steady state is a consequence of the electrode kinetics being limited by the supply of photogenerated carriers, and cannot be assigned unambiguously to a mass transport effect. Simulated cyclic voltammetry curves on band microelectrode photoanodes as a function of the photocurrent are shown in Fig. 3B. Similar to the macroelectrode photoanodes, the current density is proportional to the photocurrent, and a steady state is observed at low photocurrents.

Having developed the theoretical framework that allows us to interpret electrochemical responses of freely diffusing redox species on semiconductor microelectrodes, we then investigated the experimental response for the Fc/Fc^+ couple on LD Si(111) electrodes under local illumination. This is to demonstrate the formation of transient microelectrodes arrays with a structured light stimulus on a homogeneous substrate with a single electrical connection. A custom-built SLM device was used to project light micropatterns at the silicon–electrolyte interface (Fig. 1B). The illuminated area is expected to act as a transient electrode, able to confine in space an electrochemical reaction and to enhance mass transport. Fig. 3C shows cyclic voltammetry curves obtained when projecting lines of variable width. We chose a band geometry for our transient electrodes because it allows a broader range of currents, up to microamperes, while still retaining the microelectrode response [15]. Similar to the simulated voltammograms, the experimental curves of Fig. 3C show an increase in anodic current density as *w* gets narrower. However, and opposite to the simulated response (Fig. 3A), a steady state current is observed when *w* decreases and the cathodic current also increases. This striking contrast between simulations and experiments is probably caused by the assumption that the active electrode area is an exact match of the illumination pattern. However, equating the active area to the illuminated area is an approximation valid only when the diffusion length of the photogenerated carriers (*L*) is much smaller than the width of *w* (see schematics in Fig. 3D). If *L* is of comparable size, or bigger than *w* (Fig. 3D, right panel), one has to take into account the contribution of the photogenerated carriers diffusion length to the electrochemical current. The direct consequences of photogenerated carriers diffusing significantly outside the illuminated areas are two: 1) it leads to a wrong estimate of the active electrode area (and therefore of the current density), and 2) a distortion of the voltammetric curves. This latter point (2) is due to the anisotropic character of carriers' diffusion, and their concentration decreasing with the square of the distance, as does the local photocurrent. Consequently, the microelectrode response in Fig. 3C does not directly arise nor match the actual geometry of the illumination pattern.

In order to avoid the undesirable distortion effects mentioned in the above paragraph, we tried to adjust the overlap and separation of diffusion fronts occurring on microelectrode arrays of variable density but keeping the active area constant [21]. This can be done by generating band electrodes where the inter-band gap is systematically varied. When the bands approach each other, their diffusion fronts overlap (Fig. 4A), and the electrochemical current decreases (digital simulations of a semiconductor band microelectrode array, Fig. 4B and Section S2). In this way, the illuminated area is kept constant so that an estimation of the current density based on the active area is not necessary and effects arising from the diffusion of charge carrier effects are kept constant. By projecting band electrode patterns with different band separations as shown in Fig. 4A we were able to determine and quantify diffuse effects on our LD Si(111) photoanodes. Fig. 4C shows identical voltammetric experimental responses for an array of 8 bands (22.5 µm wide) where the inter-band gap was varied between 225 and 0 µm. A low photocurrent could limit the anodic current, but the cathodic current should show a variation with the inter-band separation current, see Fig. 4D. Further decreasing the *w* (13.5 µm) did not result in a microelectrode behaviour, Fig. S3. Therefore, as discussed above, the most likely explanation is that the electrochemical reaction is not confined exclusively in correspondence of the projected light pattern. This experiment also proves that the current difference between bands of different width shown in Fig. 3C can be unambiguously assigned to photoeffects arising when the illuminated area is decreased. The larger current density for the narrower bands arises because a wrong estimation of the electrode active area and a large *L*/*w* ratio, and a plateau is observed because the current is limited by the photogenerated charge carriers (*i.e.* is not directly related to a radial diffusion front).

3.4 Lateral diffusion of carriers as function of diffusion lengths

To confirm our hypothesis, that is, minority carriers diffusion preventing us from observing truly diffuse effects on light-activated microelectrodes, we next quantified the extent of electrochemical confinement on functionalized LD Si(111) electrodes. This was done by photoelectrochemically depositing patterns of Cu_2O: Cu^{2+} ions are reduced to Cu^{+} only where photogenerated charge carriers reach the interface, and cuprous ions then deposit as Cu_2O crystals [6, 7]. By means of imaging (ex-situ) the Cu_2O patterns, this method can be used to directly determine the mismatch between the electrochemically active area and the light pattern. For these photoelectrochemical reduction experiments we used chemically functionalized LD p-type Si(111) surfaces as a photocathode. The cyclic voltammograms of Fig. 5A show that the Cu^{2+} reduction to Cu^{+} occurs only under illumination. This is because the Cu^{2+} reduction potential lies in the depletion layer region, that is at potentials below the electrode flat-band potential (E_{fb}=−0.25 V vs Ag/AgCl/KCl sat., Mott-Schottky plot in Fig. 5B and in more details in Fig. S4). We projected 'line' patterns of different widths and compared the known width of the projected band with the width of the Cu_2O deposit estimated from scanning electron micrographs (Figs. 5C–E). As expected, the Cu_2O features extend several micrometres beyond the illuminated region, supporting a non-negligible lateral diffusion of minority carriers. A diffusion length of ca. 30–45 µm was roughly estimated by subtracting the width of the projected light feature from the actual pattern width. This value is in good agreement with previously reported values for crystalline silicon [26]. When digital simulations of cyclic voltammetry on band microelectrodes are performed taking into account this correction to the active area (Fig. S5), their agreement with the experimental results improves significantly (Fig. 4C).

To reinforce on this point – the importance of the w/L ratio in the performance and analysis of light activated microelectrodes – we tested photoelectrodes with a significantly shorter diffusion length. Amorphous silicon is a silicon allotrope with a diffusion length not exceeding few nanometres [27]. Cyclic voltammetry reveals the electrodeposition on amorphous silicon happens only under illumination (Fig. S6), and, most importantly, Cu_2O patterns accurately match (within 1 µm) the projected light feature, as shown in the SEM images of Figs. 5F–H, indicative of the short diffusion length of charge carriers in amorphous silicon.

3.5 Microelectrode arrays generated on amorphous silicon electrodes

As we have demonstrated in the previous section, for a material with a sufficiently short diffusion length, such as amorphous silicon, a photoelectrochemical reaction is confined satisfactorily within the illuminated area. Moreover, as for LD crystalline wafers, in these amorphous electrodes the Fc/Fc^{+} redox reaction happens only under illumination (Fig. S7) [28]. Therefore, amorphous silicon should be an ideal substrate to gain enhanced mass transport by forming microelectrode arrays with light. Fig. 6A are voltammograms obtained on amorphous silicon photoelectrodes when projecting arrays of light bands with changes to the inter-band separation. These data show an increase of the electrochemical current and a progressive loss of the voltammograms hysteresis as the bands are progressively separated, both indicating an effective separation of the diffusion fronts, hence a more efficient mass transport to the electrode leading to a true stationary of quasi-stationary behaviour [15]. Fig. 6B shows the effect of changes to the scan rate for the band microelectrode array. As expected for microelectrodes, the scan rate has little effect on the electrochemical current for the case of isolated microband electrodes since a pseudo-stationary state has been attained under these conditions. We note that the current–potential curves in Fig. 6A and B show a clear distortion of the current–potential shape. Moreover, the appearance of a shift towards more positive potentials, which for the curves in Figs. 6A is of 65 mV for the half-wave potential (see Fig. S8), is a typical feature of non-reversible redox processes, but finite kinetics factors can be here discarded due to the practically null shift of the voltammograms with the scan rate (Fig. 6B). Thus, a cause of this distortion could be ohmic factors since this distortion is more evident as the current increases (see also Fig. S7 corresponding to a macroelectrode which clearly shows a distorted voltammogram as compared with an ohmic-free current–potential curve). That is, although the increase in current can be directly related to a "pure" mass transport effect, a quantitative evaluation of the observed behaviour should include an ohmic drop contribution to the applied potential. This refinement to the analytical models will be the subject of a future work.

4. Conclusion

We have shown that transient microelectrode arrays can be formed on an unstructured semiconductor substrate by projecting light patterns of user-defined size and geometry. Enhanced mass transport to the electrode surface was demonstrated by separating the diffusion fronts feeding the active areas of transient (light-addressed) microelectrode band arrays. This method allows to differentiate between true microelectrode response (due to radial mass transport), and apparent microelectrode response (due to distortion of the voltammograms at high ratios of diffusion length to width of the illuminated area). The cautionary note is that steady state currents are not necessarily indicating efficient mass transport, but can instead be a consequence of the electrode kinetics being limited by the supply of photogenerated carriers. We have defined the influence of the diffusion length on the photoelectrochemical responses of these transient microelectrodes by comparing two different silicon allotropes of very different carriers' diffusion length. Ideal microelectrode responses are achievable in amorphous silicon, but not in crystalline silicon. This is due to an enhanced electrochemical confinement ensured in amorphous silicon by a short (few nanometres) diffusion length. We have developed an analytical model to account for microelectrode geometry and for the splitting of the potential applied at the semiconductor–electrolyte solution into two contributions: a diode–solution and a metal–solution potential drops. The theoretical description of the influence of light intensity, separation between band electrodes and scan rates, qualitatively agrees with the experimental data, yielding deeper physical insights on the process of guiding electrochemical activity at semiconductors with spatially structured light.

Transient microelectrode arrays created using a spatial light modulator and unstructured macroscopic photoconductors, or semiconductors, can be a tool for chemical analysis with performances comparable to those of conventional microelectrodes [29], but with the advantage of lifting almost entirely geometrical restrictions on the active area.

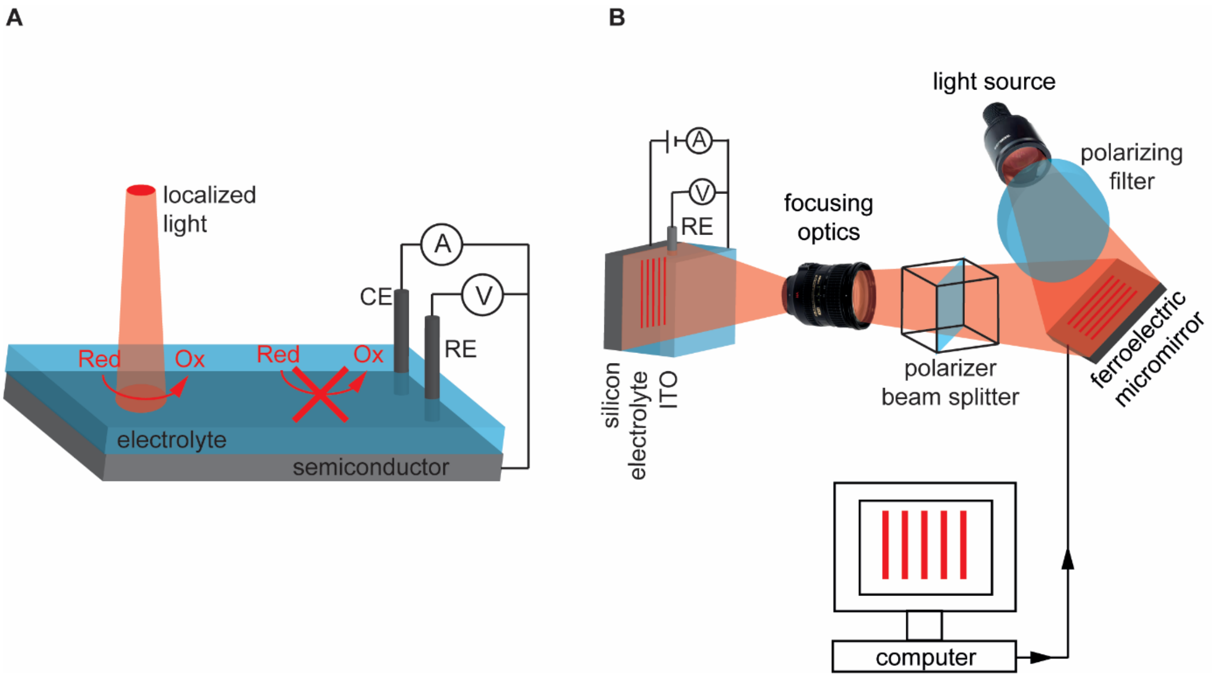

Fig. 1. Microelectrode arrays with active-area geometries defined by spatial light modulation (A) Depiction of the light-activated electrochemistry principle at a depleted semiconductor–electrolyte interface. (B) Schematics of the ferroelectric liquid crystal on silicon spatial light modulator (SLM) used to project light micropatterns at the silicon–electrolyte interface.

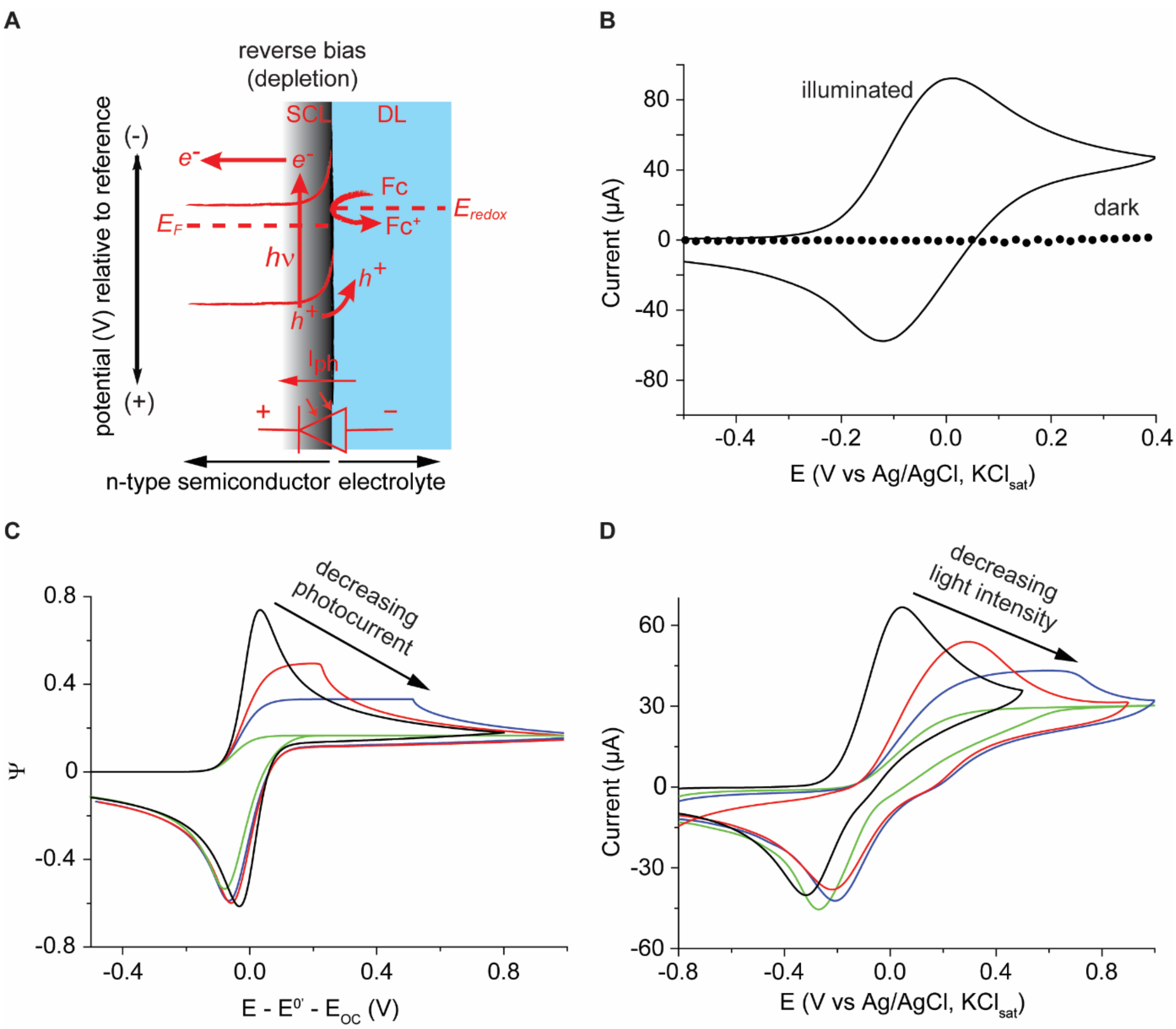

Fig. 2. Electrochemical switching by a light stimulus and cyclic voltammetry of freely diffusing redox species on a photoanode

(A) Representation of the potential profile across an n-type semiconductor–liquid interface and its photoelectrochemistry under reverse bias. (B) Cyclic voltammograms of ferrocene (Fc, 1.0 $\times 10^{-3}$ M) under illumination (solid line) and dark (dotted line) acquired on a functionalized LD n-type Si(111) electrode (0.1 V/s, 0.1 M Bu_4NClO_4 in acetonitrile). (C) Simulated cyclic voltammograms (equations (24-25) of the supplementary information, 0.1 V/s) for a semiconductor photoanode under variable photocurrents (I_L = 25, 3, 2 and 1 μA, black, red, blue and green lines, respectively, see Section S2) and assuming completely reversible electron transfer kinetics. For the simulations, the diffusion coefficient was set to 1.0×10^{-5} cm^2/s, the reverse saturation current (leakage) to 1.0×10^{-5} μA, and the bulk concentration of Fc to 1.0×10^{-3} M. (D) Experimental cyclic voltammograms of Fc solutions in acetonitrile (1.0×10^{-3} M Fc, 0.1 M Bu_4NClO_4, and sweep rate of 0.1 V/s) recorded on a chemically modified LD n-type Si(111) electrode under variable illumination intensities (1030, 170, 100 and 80 klux). The current axis in the simulated voltammograms has been normalized to the dimensionless current ψ (Section S2) and the abscissa represents the voltage, E, relative to the redox formal potential, $E^{0'}$, corrected for the open-circuit potential, E_{OC} (i.e., $E - E^{0'} - E_{OC}$).

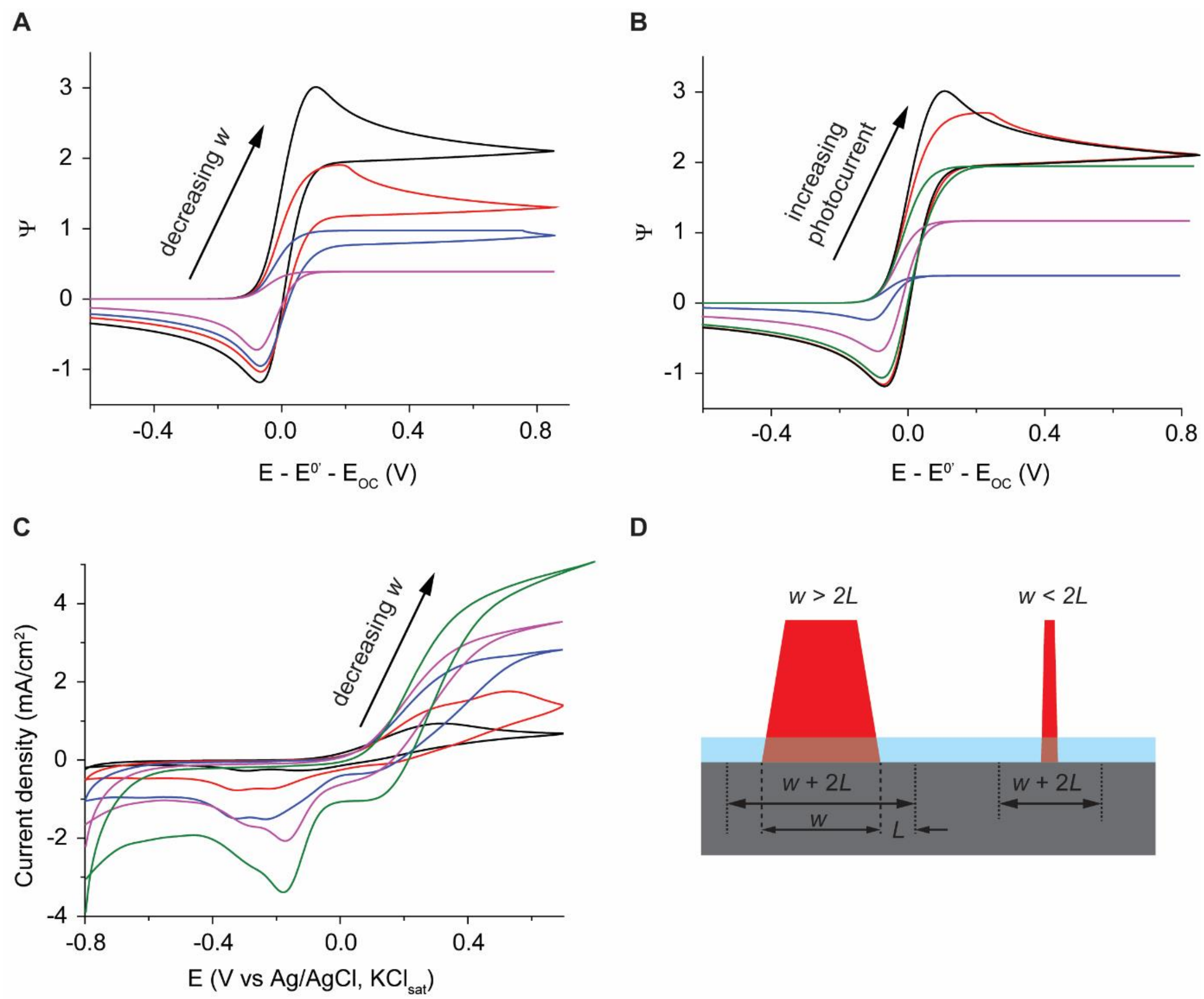

Fig. 3. Voltammetric photocurrent–potential behaviour of freely diffusing Fc/Fc^+ on Si(111) electrodes under local illumination. (A) Simulated cyclic voltammograms (equations (24–25) of the supplementary information, voltage sweep rate of 0.01 V/s) for a band semiconductor microelectrode as a function of its width (*w*, 22.5, 45, 90 and 225 µm). The photocurrent is 10 µA. (B) Simulated cyclic voltammograms (equations (24–25) of the supplementary information, 0.01 V/s) for a band semiconductor microelectrode as a function of the photocurrent. The photocurrents are 10, 7, 5, 3 and 1 µA. *w* is 22.5 µm. For the simulations a diffusion coefficient of 10^{-5} cm^2/s, an initial concentration of 10^{-3} M of reduced species, and a reverse saturation current of 10^{-5} µA were used. (C) Experimental cyclic voltammograms (0.01 V/s) of ferrocene solutions on a chemically modified LD n-type Si(111) electrode under local illumination. A line-shaped (band) of specific width (22.5, 45, 90, 225 and 450 µm) was projected on the interface. Cyclic voltammograms were recorded in acetonitrile with 0.1 M Bu_4NClO_4 and 1.0 × 10^{-3} M of ferrocene. (D) Schematics of the silicon–electrolyte interface under localized illumination (red area). The ratio of the width of the illuminated area (*w*) to the diffusion length (*L*) is the key parameter to understand and predict the electrochemical behavior under local illumination of a semiconductor electrode. As *w* decreases, and becomes comparable to, or smaller than 2*L*, carriers diffusing away from the generation site become the main contributors to the electrochemical current, and have therefore to be accounted for.

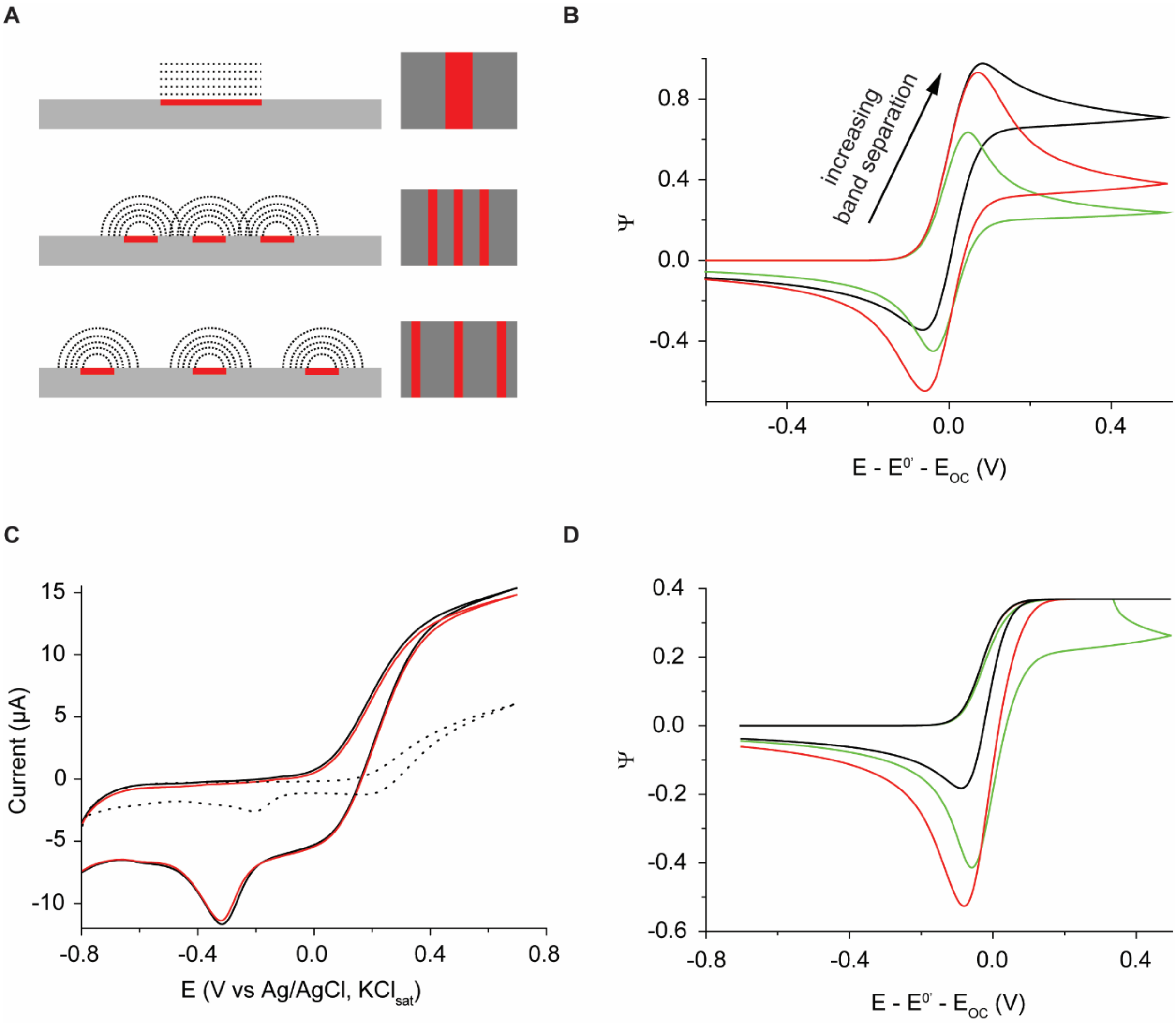

Fig. 4. Cyclic voltammetry of light-addressed microelectrode band arrays on crystalline silicon. (A) Schematics representing the diffusion fronts of a microelectrode band array. (B) Simulated cyclic voltammograms (equations (24–25) of the supplementary information, voltage sweep rate is 0.1 V/s) for an array of semiconducting band microelectrodes as a function of the inter-band separation. The inter-band separations are 112.5 (black line), 11.25 µm (red line) and 0.225 µm (green line). The photocurrent is set to 5 µA. (C) Experimental voltammograms (0.1 V/s) recorded when projecting arrays of 22.5 µm wide line-shaped bands separated by gaps of 225 µm (red line) or 0 µm (black line). Dotted data were obtained under dark conditions. Chemically modified LD n-type Si(111) surfaces were used as the working electrode. The electrolyte was acetonitrile with 0.1 M Bu_4NClO_4 and 1.0×10^{-3} M ferrocene. (D) Simulated cyclic voltammograms ((equations (24–25) of the supplementary information, 0.1 V/s) for an array of semiconducting band microelectrodes as a function of the inter-band separation. Separations are 112.5 (black line), 11.25 µm (red line) and 0.225 µm (green line). The photocurrent is set to 1 µA, the diffusion coefficient to 1.0×10^{-5} cm^2/s, the concentration of reducible species to 1×10^{-3} M, and the reverse saturation current to 1.0×10^{-5} µA.

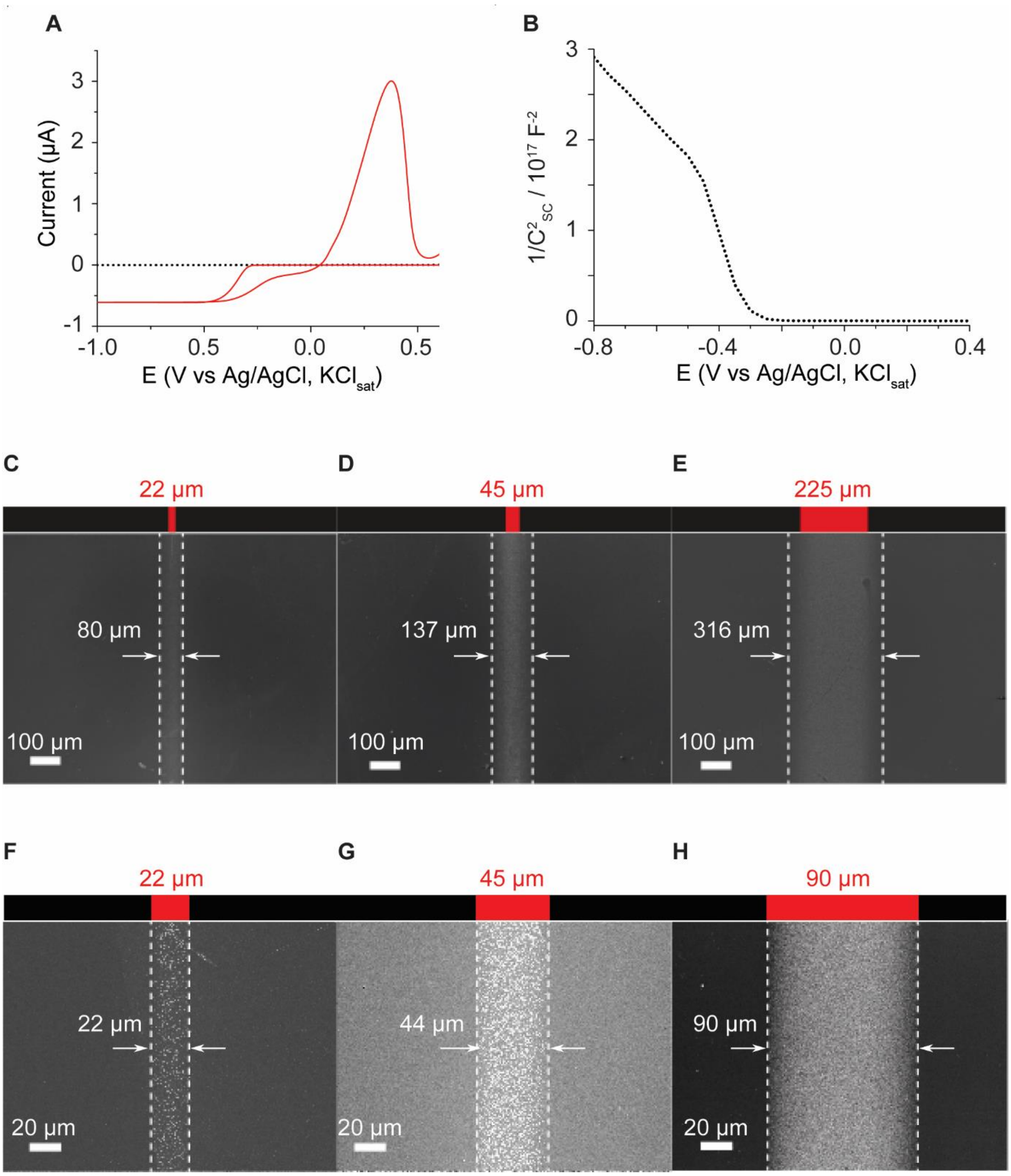

Fig. 5. Lateral diffusion as function of diffusion lengths. Redox mask-free lithography on silicon (Cu_2O patterns). (A) Cyclic voltammetry (0.1 V/s) under dark (symbols) and light (solid line) on alkyne modified LD p-Si(100) electrodes. (B) Mott-Schottky plot used to estimate the flat-band potential for the alkyne modified LD p-Si(100) electrodes. (C)–(H) Scanning electron microscopy images of Cu_2O patterns deposited on either crystalline silicon (C)–(E), or on amorphous silicon (F)–(H). Patterns were formed by projecting on the electrode a line-shaped light feature of width specified by the red ink labels placed above the micrographs. The experimental width of the Cu_2O pattern is specified by the white ink labels. The electrolyte was an aqueous solution of $5.0 \times \cdot 10^{-2}$ M of $CuSO_4$ and 0.5 M of K_2SO_4. The total charge transferred per unit of illuminated area was kept constant (1 $\mu C \cdot \mu m^{-2}$). The electrodeposition potential was stepped from the open circuit to a potential of −0.5 V.

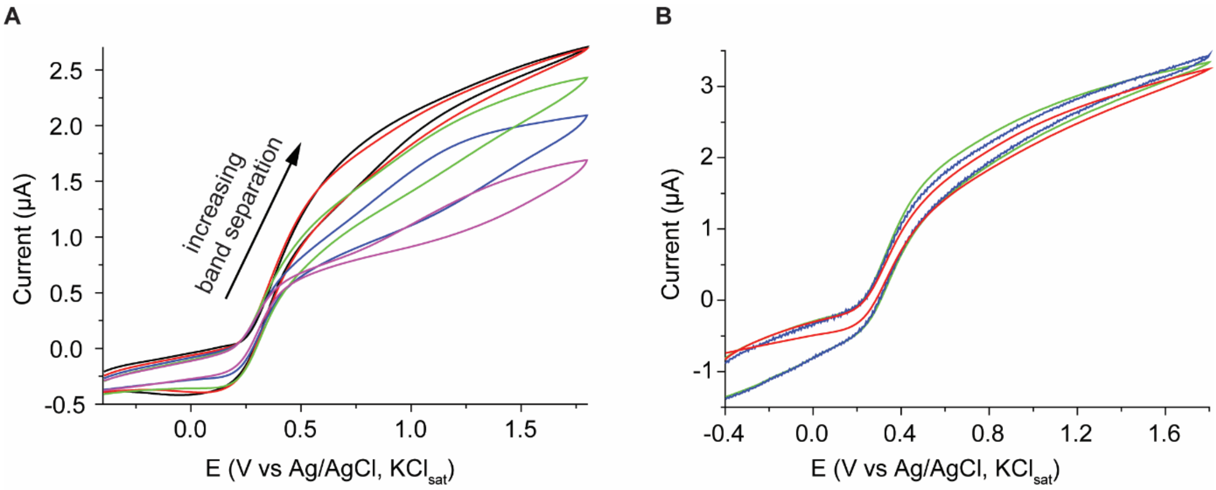

Fig. 6. Microelectrode arrays generated on amorphous silicon electrodes. Forming transient microelectrodes arrays with light in a material with short charge carriers' diffusion length. (A) Experimental cyclic voltammograms (0.1 V/s) of ferrocene solutions when projecting an array of 13.5 µm wide light bands with variable inter-band separation (270, 135, 68, 27 and 0 µm, shown as black, red, green, blue and magenta solid lines, respectively). (B) Experimental voltammetry of ferrocene at different voltage scan rates (0.3, 0.05 and 0.025 V/s, shown as green, blue and red solid lines, respectively) when projecting a fixed band array (13.5 µm band width and band separation of 270 µm). Chemically modified amorphous silicon was used as the working electrode and the electrolyte is 0.1 M Bu_4NClO_4 in acetonitrile with 1.0×10^{-3} M ferrocene.

Authors' contributions

S.C., J.G. and Y.B.V conceived and designed the research. Y.B.V. performed the experiments, analyzed and visualized the data, with assistance from J.G. and A.M. Codes for the digital simulations of the voltammetry were developed, written and executed by J.G., with assistance from A.M.. All authors contributed to the writing and editing of the manuscript.

Declaration of competing interest

The authors declare that they have no known competing financial interests or personal relationships that could have appeared to influence the work reported in this paper.

Acknowledgements

This work was supported by the Australian Research Council (DP190100735 and FT190100148 (S.C.)). J.G. and A.M. greatly appreciate the financial support provided by the Fundacion Séneca de la Región de Murcia (Project 19887/GERM/15).

Supplementary materials

Supplementary material associated with this article can be found in the online version.

References

[1] S. Singh-Gasson, R.D. Green, Y. Yue, C. Nelson, F. Blattner, M.R. Sussman, F. Cerrina, Maskless fabrication of light-directed oligonucleotide microarrays using a digital micromirror array, Nat. Biotechnol., 17 (1999) 974–978.

[2] V. Nikolenko, B. Watson, R. Araya, A. Woodruff, D. Peterka, R. Yuste, SLM microscopy: Scanless two-photon imaging and photostimulation using spatial light modulators, Front. Neural Circuits, 2 (2008).

[3] B.E. Kelly, I. Bhattacharya, H. Heidari, M. Shusteff, C.M. Spadaccini, H.K. Taylor, Volumetric additive manufacturing via tomographic reconstruction, Science, 363 (2019) 1075-1079.

[4] C. Lutz, T.S. Otis, V. DeSars, S. Charpak, D.A. DiGregorio, V. Emiliani, Holographic photolysis of caged neurotransmitters, Nat. Methods, 5 (2008) 821-827.

[5] Y.B. Vogel, J.J. Gooding, S. Ciampi, Light-addressable electrochemistry at semiconductor electrodes: redox imaging, mask-free lithography and spatially resolved chemical and biological sensing, Chem. Soc. Rev., 48 (2019) 3723-3739.

[6] Y.B. Vogel, N. Darwish, M.B. Kashi, J.J. Gooding, S. Ciampi, Hydrogen evolution during the electrodeposition of gold nanoparticles at Si(100) photoelectrodes impairs the analysis of current-time transients, Electrochim. Acta, 247 (2017) 200-206.

[7] Y.B. Vogel, V.R. Gonçales, L. Al-Obaidi, J.J. Gooding, N. Darwish, S. Ciampi, Nanocrystal inks: Photoelectrochemical printing of Cu_2O nanocrystals on silicon with 2D control on polyhedral shapes, Adv. Funct. Mater., 28 (2018) 1804791.

[8] Y.B. Vogel, J. Zhang, N. Darwish, S. Ciampi, Switching of current rectification ratios within a single nanocrystal by facet-resolved electrical wiring, ACS Nano, 12 (2018) 8071-8080.

[9] D.-W. Zhang, N. Papaioannou, N.M. David, H. Luo, H. Gao, L.C. Tanase, T. Degousée, P. Samorì, A. Sapelkin, O. Fenwick, M.-M. Titirici, S. Krause, Photoelectrochemical response of carbon dots (CDs) derived from chitosan and their use in electrochemical imaging, Mater. Horiz., 5 (2018) 423–428.

[10] Y.B. Vogel, V.R. Gonçales, J.J. Gooding, S. Ciampi, Electrochemical microscopy based on spatial light modulators: A projection system to spatially address electrochemical reactions at semiconductors, J. Electrochem. Soc., 165 (2018) H3085-H3092.
[11] S.G. Parker, Y. Yang, S. Ciampi, B. Gupta, K. Kimpton, F.M. Mansfeld, M. Kavallaris, K. Gaus, J.J. Gooding, A photoelectrochemical platform for the capture and release of rare single cells, Nat. Commun., 9 (2018) 2288.
[12] J. Suzurikawa, M. Nakao, R. Kanzaki, H. Takahashi, Microscale pH gradient generation by electrolysis on a light-addressable planar electrode, Sens. Actuators, B, 149 (2010) 205-211.
[13] M.H. Choudhury, S. Ciampi, Y. Yang, R. Tavallaie, Y. Zhu, L. Zarei, V.R. Goncales, J.J. Gooding, Connecting electrodes with light: One wire, many electrodes, Chem. Sci., 6 (2015) 6769-6776.
[14] C.N. LaFratta, D.R. Walt, Very high density sensing arrays, Chem. Rev., 108 (2008) 614-637.
[15] D. Li, C. Batchelor-McAuley, L. Chen, R.G. Compton, Band electrodes in sensing applications: Response characteristics and band fabrication methods, ACS Sensors, 4 (2019) 2250-2266.
[16] R.J. Forster, Microelectrodes: New dimensions in electrochemistry, Chem. Soc. Rev., 23 (1994) 289–297.
[17] P.G. Santangelo, G.M. Miskelly, N.S. Lewis, Voltammetry of semiconductor electrodes. 2. Cyclic voltammetry of freely diffusing redox species and rotating semiconductor disk voltammetry, J. Phys. Chem., 93 (1989) 6128–6136.
[18] S. Ciampi, T. Böcking, K.A. Kilian, M. James, J.B. Harper, J.J. Gooding, Functionalization of acetylene-terminated monolayers on Si(100) surfaces: A click chemistry approach, Langmuir, 23 (2007) 9320-9329.
[19] S. Ciampi, P.K. Eggers, G. Le Saux, M. James, J.B. Harper, J.J. Gooding, Silicon (100) electrodes resistant to oxidation in aqueous solutions: An unexpected benefit of surface acetylene moieties, Langmuir, 25 (2009) 2530-2539.
[20] A.J. Bard, L.R. Faulkner, J. Leddy, C.G. Zoski, Electrochemical Methods: Fundamentals and Applications, Wiley, New York, 1980.
[21] R.G. Compton, C.E. Banks, Understanding Voltammetry, World Scientific2011.
[22] Y.B. Vogel, A. Molina, J. Gonzalez, S. Ciampi, Quantitative analysis of cyclic voltammetry of redox monolayers adsorbed on semiconductors: Isolating electrode kinetics, lateral interactions, and diode currents, Anal. Chem., 91 (2019) 5929–5937.
[23] P.G. Santangelo, G.M. Miskelly, N.S. Lewis, Cyclic voltammetry at semiconductor photoelectrodes. 1. Ideal surface-attached redox couples with ideal semiconductor behavior, J. Phys. Chem., 92 (1988) 6359–6367.
[24] P.G. Santangelo, M. Lieberman, N.S. Lewis, Cyclic voltammetry of semiconductor photoelectrodes III: A comparison of experiment and theory for n-Si and p-Si electrodes, J. Phys. Chem. B, 102 (1998) 4731–4738.
[25] Y.B. Vogel, L. Zhang, N. Darwish, V.R. Gonçales, A. Le Brun, J.J. Gooding, A. Molina, G.G. Wallace, M.L. Coote, J. Gonzalez, S. Ciampi, Reproducible flaws unveil electrostatic aspects of semiconductor electrochemistry, Nat. Commun., 8 (2017) 2066.
[26] M. George, W.J. Parak, I. Gerhardt, W. Moritz, F. Kaesen, H. Geiger, I. Eisele, H.E. Gaub, Investigation of the spatial resolution of the light-addressable potentiometric sensor, Sens. Actuators, A, 86 (2000) 187-196.
[27] W. Moritz, T. Yoshinobu, F. Finger, S. Krause, M. Martin-Fernandez, M.J. Schöning, High resolution LAPS using amorphous silicon as the semiconductor material, Sens. Actuators, B, 103 (2004) 436-441.
[28] V.R. Gonçales, J. Lian, S. Gautam, D. Hagness, Y. Yang, R.D. Tilley, S. Ciampi, J.J. Gooding, Heterojunctions based on amorphous silicon: A versatile surface engineering strategy

to tune peak position of redox monolayers on photoelectrodes, J. Phys. Chem. C, 124 (2020) 836-844.
[29] M. Lancaster, A. AlQurashi, C.R. Selvakumar, S. Maldonado, Quantitative analysis of semiconductor electrode voltammetry: A theoretical and operational framework for semiconductor ultramicroelectrodes, J. Phys. Chem. C, 124 (2020) 5021-5035.